Cerebral Cortex, 2024, **34**, 1–14
https://doi.org/10.1093/cercor/bhad517
Advance access publication date 6 January 2024
Original Article

Neural response properties predict perceived contents and locations elicited by intracranial electrical stimulation of human auditory cortex

Qian Wang

Received: June 16, 2023. **Revised:** December 9, 2023. **Accepted:** December 10, 2023

that auditory cortical sites with iES-elicited hallucinations and those with iES-elicited illusions exhibit distinct anatomical distributions (De Graaf et al. 2000; Howard et al. 2000; Hamilton et al. 2021; Trébuchon et al. 2021). However, other studies have reported overlapping distributions of hallucination and illusion sites within the auditory cortex (Fenoy et al. 2006; Jaroszynski et al. 2022). These inconsistent findings make it challenging to create a uniform anatomical distribution map of subjective sound experiences, rendering iES-elicited percepts unpredictable. Therefore, a more direct method to examine this assumption involves determining if any intrinsic response signatures can predict the perceived contents and locations of iES-elicited percepts; however, there is currently a lack of empirical evidence in this regard.

To investigate whether neuronal populations that engage in distinct iES-elicited percepts encode and represent sound information differently, we combined iES and intracranial electroencephalogram (iEEG) approaches in the human auditory cortex with high spatiotemporal precision. In the current study, we classified the cortical sites based on the contents and locations of iES-elicited sound experiences and then extracted which critical neuronal properties from iEEG signals can predict the type of iES-elicited percepts. The iES approach enabled us to reveal perceived contents and locations of the internal sound experience when a neuronal population around an electrode site was stimulated. Meanwhile, the iEEG approach elucidated how the same neuronal population encodes and represents external acoustic stimuli. The combination of these two approaches provided a rare and unique opportunity to explore the relationship between intrinsic neuronal properties and perceived content and location (Schrouff et al. 2020; Wang et al. 2020; Hamilton 2022).

Materials and methods

Participants

A cohort of 28 patients (10 females, age range 13–43 yr) with drug-resistant epilepsy who underwent invasive stereo-electroencephalogram monitoring for potential surgical interventions at the Sanbo Brain Hospital of Capital Medical University (Beijing, China) were recruited. All patients were native Chinese speakers. Patient selection criteria required the presence of at least one electrode implanted in the superior temporal gyrus. All participants were right-handed and self-reported normal hearing, and provided written informed consent for their participation. The study procedures were approved by the Ethics Committee of the Sanbo Brain Hospital of Capital Medical University and the Human Subject Review Committee of Peking University. Details of patient demographics are provided in Table 1.

Stereo-electrode site localization and selection

All 28 patients were implanted with stereo-electrodes. In total, 8–20 electrodes were implanted in total for each patient. Each stereo-electrode had 8–16 sites (0.8 mm in diameter, 2 mm in length, spacing 3.5 mm apart; Huake Hengsheng Medical Technology Co. Ltd, Beijing, China). The electrode implantations were determined based on clinical reasons. For stereo-electrode site localization, the post-implantation computed tomograph (CT) images were co-registered with the pre-implantation T1-weighted magnetic resonance imaging (MRI) scans for each subject using the SPM12 toolbox (available at https://www.fil.ion.ucl.ac.uk/spm/software/spm12/) (Penny et al. 2011). Then, we identified individual electrodes on the aligned CT images and calculated the coordinates of electrode sites using the Brainstorm toolbox (available at http://neuroimage.usc.edu/brainstorm) (Tadel et al. 2011). Three-dimensional brain surfaces were reconstructed by pre-implantation MRI (T1-weighted or contrast-enhanced) and registered to the University of Southern California (USC) Brain atlas (Joshi et al. 2022) using the BrainSuite software (http://brainsuite.org/). The localization of each site was identified using the individual atlas of each patient. The sites localized in the Heshl's gyrus (HG), middle superior temporal gyrus (mSTG), and posterior superior temporal gyrus (pSTG), were selected as auditory cortical sites. For visualization, we computed MNI coordinates of each site individually and displayed them on a cortical template (ICBM152). The sites with over-threshold impedances (>50 kΩ), electromagnetic artifacts, and/or within epilepsy foci were excluded from data analyses based on visual inspection.

Intracranial electrical stimulation

All patients underwent iES mapping as part of a routine clinical procedure to determine essential sensory, motor, and other cognitive function using Nicolet® Cortical Stimulator (Natus Neuro, USA). In each iES trial, a train of biphasic electrical pulses (square-wave, 0.5–6 mA, 50 Hz, 200-μs pulse width, 5-s duration) was delivered to pairs of adjacent sites. During the iES procedure, patients were asked to perform a number counting task (speak loudly from one to one hundred) and to report immediately if they had any feelings. Patients were unaware of the timing of the stimulation and the anatomical location of the stimulation sites. Patients' self-reports were reviewed and further classified by an experienced neuropsychologist (Dr Jing Wang) (see details in Supplementary Table 1). We considered the anode of the electrical stimulation as the focal point of the iES procedure, thereby aligning it with the location of the iEEG recording site.

iEEG recording

Intracranial EEG signals were recorded at a sampling rate of 512 Hz using a Nicolet video-EEG monitoring system (Thermo Nicolet Corp., USA) without any online filtering. Both the reference and ground electrodes were placed at the forehead of the patients. All further processing was performed offline.

To obtain the sound-induced responses, we recorded intracranial signals via stereo-electrode sites when patients were passively listening to Gaussian wideband noise bursts. The wideband-noise stimulus was synthesized in MATLAB environment (MathWorks, Natick, MA, USA) at the sampling rate of 48 kHz with 16-bit amplitude quantization and low-pass filtered at 10 kHz. The duration of the noise burst stimulus was 50 ms including the 5-ms linear ramp and damp. The interstimulus interval (ISI) randomly varied between 900 and 1100 ms. The acoustic stimulus was transferred using Creative Sound Blaster X-Fi Surround 5.1 Pro (Creative Technology Ltd, Singapore) and presented to patients with insert earphones (ER-3, Etymotic Research, Elk Grove Village, IL) at the sound pressure level of 65 dB SPL. Calibration of the sound level was carried out with the Larson Davis Audiometer Calibration and Electroacoustic Testing System (AUDit and System 824, Larson Davis, Depew, NY).

All patients were presented with binaural noise bursts (180 trials), and 22 patients (P236-P421) were additionally presented with ipsilateral (160 trials) and contralateral (160 trials) noise bursts. Patients were reclining in a ward in the hospital during the experiment. The experimental procedure was suspended for at least 2 h after a seizure (if there was any), to avoid the seizure-induced cortical suppression effect. At the beginning of each trial, we transmit an analog signal to the iEEG recording system. This step is crucial to ensure synchronization with the sound stimulation system.

Table 1. Patients' demographic and clinical data.

Patient#	Age	Sex	Implanted hemisphere	Count of selected sites
121	24	F	L	4
172	30	F	R	4
206	26	M	L	3
207	28	M	R	3
220	26	M	L	3
229	28	M	R	8
236	18	M	R	2
240	29	F	L	1
243	27	M	R	4
263	28	M	L	5
272	31	M	R	3
276	20	M	L	1
280	23	M	L, R	9
281	31	F	L	2
282	27	F	L	5
290	26	M	L, R	4
361	27	F	R	3
365	27	M	L	3
370	25	F	L, R	11
373	15	M	R	6
381	27	F	L	1
386	29	M	L, R	2
409	21	M	R	4
412	29	M	L	4
413	43	F	L	6
414	31	M	L	5
419	34	N	R	5
421	13	F	L	2
Sum				113

F, female; M, male; L, left; R, right.

Preprocessing of iEEG signals

All the intracranial signals were pre-processed using the EEGLAB toolbox (Delorme and Makeig, 2004) in the MATLAB environment. The continuous signals were then segmented into epochs from −100 to 600 ms around the sound onset and normalized to the baseline (−100 to 0 ms) using the *pop_rmbase* function. The epochs that contained interictal discharges or movement artifacts were rejected, as confirmed by visual inspection.

Time-frequency analyses

Time-frequency analyses were performed on the epoched signal using continuous Morlet wavelet transformation (function *cwt*) in Matlab. For each electrode site, time-frequency maps with a frequency range from 2 to 180 Hz and a time range from −50 to 300 ms were calculated for each trial. The amplitudes of the time-frequency maps were then averaged across trials. Paired *t*-tests were performed point-by-point to compare the time-frequency components between two conditions. Significant time-frequency points ($P < 0.005$, two-tailed) were then clustered based on spatial adjacency, with a minimum of ten adjacent points to form a cluster. We use the FDR method to correct the multiple comparison. The temporal profiles in the high-γ band (60–140 Hz) and the alpha band (6–14 Hz) activities were subs11.8.3(s)-.3(h)-418y7(of)-deo

For NMF clustering results, to quantify the relative contribution of the transient and sustained components, we calculated a relative weight as:

$$relative\ weight = \frac{W_T - W_S}{W_T + W_S} \quad (3)$$

The resulting relative weight ranges from −1 to 1. The categorization of a specific site as either sustained or transient was determined through the utilization of the relative weight value. Specifically, if the relative weight value was found to be less than zero, the site was classified as sustained. Conversely, if the relative weight value exceeded zero, the site was designated as transient. A higher relative weight value indicates a more transient property.

Spectra-temporal decoding

Based on the iES-elicited percepts, we divided the electrode sites into four groups: contralateral hallucination ($n = 43$), bilateral hallucination ($n = 8$), contralateral illusion ($n = 18$), and bilateral illusion ($n = 8$) (Fig. 6). For each site, we built two models using the spectra-temporal features in the high-γ band (60–140 Hz) or those in the α band (6–14 Hz), respectively, to classify the neural activities induced by ipsilateral and contralateral sounds. We employed a support vector machine (SVM) approach for each model using single-trial spectra-temporal features (Xu et al. 2023).

The spectra-temporal features were extracted from 52 bins [13 spectra-steps × 4 temporal-steps] of single-trial time-frequency amplitude maps in the high-γ band or those in the α band. A given spectra-temporal feature equals the averaged time-frequency amplitude in a corresponding bin. All SVM analyses were performed in MATLAB using functions from the LIBSVM toolbox (Chang and Lin 2011; https://www.csie.ntu.edu.tw/~cjlin/libsvm/). For each site, the decoding accuracy of the high-γ band model and that of the α band model were obtained, respectively. The SVM model utilized the radial basis function (RBF) kernel with two parameters: Gamma and C, as described by Hsu et al. (2003). We optimized these parameters through a grid search in conjunction with the leave-one-out cross-validation technique. We evaluated various pairs of (Gamma, C) values, ranging exponentially from 2–10 to 210 in increments of 20.5. The parameter pair yielding the highest cross-validation accuracy was chosen. Parameters were selected using only the training and not testing data set to avoid overfitting risk. To test the significance of the decoding accuracy, we compared the observed decoding accuracy with a null distribution generated by permutation (swapping trial labels before SVM training) 1,000 times.

Binary logistic regressions

To assess the potential predictive capability of neural response characteristics in relation to the contents and locations perceived elicited by iES, we performed binary logistic regression analyses. These analyses were designed to explore the association between each neural index and our binary classification of electrode sites (designated as "Percept A" or "Percept B"). The latter was used as the dependent variable, as depicted in Fig. 1C. We conducted these analyses using IBM SPSS Statistics 22 software (SPSS, Chicago, IL, USA).

Statistical analyses

Statistical analyses were performed with IBM SPSS Statistics 22 software (SPSS, Chicago, IL, USA). Paired *t*-tests, independent-samples *t*-tests, chi-square tests, analyses of variance (ANOVAs), and post hoc comparisons (with *Bonferroni* corrections) tests were conducted. The null hypothesis rejection level was set at 0.05.

Results

We collected first-person reports elicited by iES applied to 3062 intracranial sites in 28 epileptic patients who underwent stereo-electrode implantation to identify the source of their seizure onset zones. The iES procedure was conducted by clinicians who were blinded to the study's objectives, and the first-person reports were recorded on paper. The reports were examined and screened by an experienced neurologist (Dr Jing Wang). Our analysis revealed that subjective reported effects were found in 1,316 sites (42.98%). Among these sites, 153 exhibited iES-elicited auditory percepts, which were referred to as auditory elicitation sites. We then identified 113 auditory elicitation sites located in the auditory cortex, including HG ($n = 79$), middle superior temporal gyrus (mSTG, $n = 16$), and posterior superior temporal gyrus (pSTG, $n = 18$). According to previous studies, HG encompasses the major part of the primary auditory cortex, while mSTG and pSTG are considered mostly as non-primary auditory cortex (Clarke and Morosan 2012; O'Sullivan et al. 2019).

We classified auditory elicitation sites based on the perceived contents and locations elicited by iES. We identified two subsets of auditory elicitation sites: hallucination ($n = 77$) and illusion ($n = 36$) sites (Fig. 1A), with hallucinations defined as generative perceptions of sounds that do not exist acoustically, and illusions defined as altered perceptions of sounds that do exist acoustically. Most of the hallucination sites exhibited simple sound contents ($n = 74$), while three sites exhibited complex sound contents such as familiar music and songs (Trébuchon et al. 2021; Jaroszynski et al. 2022). Illusion sites were further divided into suppression ($n = 12$) and echo ($n = 24$) sites (Fenoy et al. 2006; Jaroszynski et al. 2022). As shown in Fig. 1A, we classified auditory elicitation sites based on their perceived locations, with most hallucination ($n = 53$) and illusion ($n = 22$) sites exhibiting perceived locations contralateral to their iES sides. A small subset of hallucination ($n = 13$) and illusion ($n = 8$) sites exhibited perceived locations bilaterally (e.g. "'Cheep' sounds in both ears appear."). Patients failed to report the exact perceived locations of the iES-elicited auditory percepts in 17 sites (hallucination, $n = 11$; illusion, $n = 6$). All the perceived contents and locations that we observed in the current study have been reported in previous studies (Fenoy et al. 2006; Leonard et al. 2016; Sani et al. 2018; Trébuchon et al. 2021; Jaroszynski et al. 2022).

In addition to the iES procedure, patients also underwent a passive listening task during which their iEEG signals were continuously recorded (Fig. 1B). Binaural white noises were presented to all 28 patients and the sound-induced iEEG signals were analyzed to investigate the intrinsic response properties of the neuronal population surrounding each site. In order to explore how auditory space was represented by the neuronal population around each site, 22 patients (P236-P421) were presented with ipsilateral and contralateral sounds.

Sound-induced high-γ band signatures predicted perceived contents elicited by iES

We explored the anatomical distribution of hallucination and illusion sites. Figure 2B shows that more hallucination (72.70%) and illusion (63.9%) sites were localized in HG, with relatively smaller proportions localized in mSTG and pSTG. Regarding the proportions of hallucination sites and illusion sites, there was no significant difference among HG, mSTG, and pSTG ($\chi 2\ (2) = 1.590$; $P = 0.452$). However, we observed a hemispheric asymmetry, with more illusion sites localized in the left hemisphere (69.4%) ($\chi 2\ (1) = 6.941$; $P = 0.008$) (Jaroszynski et al. 2022).

We proceeded to compare the time-frequency map (ranging from 0 to 180 Hz; −50 to 300 ms) of the sound-induced responses

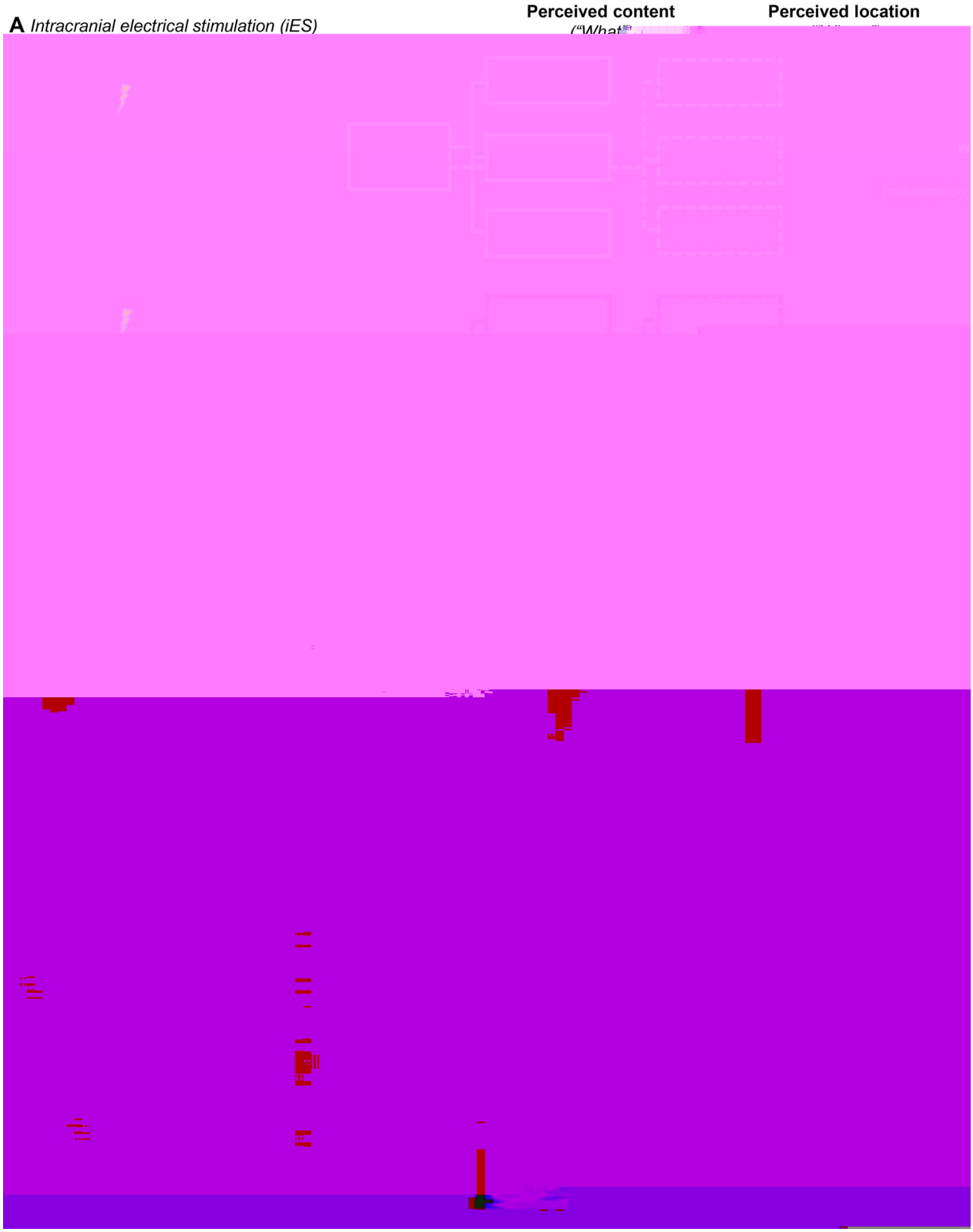

Fig. 1. Experimental procedures and regression model. (A) Schematic illustration of the iES procedure (*left*) and the tree diagram of the classification of iES-elicited auditory percepts (*right*). *Black dialog boxes* present two representative self-reports of iES-elicited auditory percepts. *Red boxes* indicate hallucinations. *Blue boxes* indicate illusions. *Solid boxes* represent the classification based on perceived contents. *Dashed boxes* represent the classification based on perceived locations. (B) Schematic illustration of the iEEG procedure (*left*), sound-induced responses (*middle*), and the time-frequency map of a representative sound-induced response (*right*). (C) Schematic illustration of the binary logistic regression model.

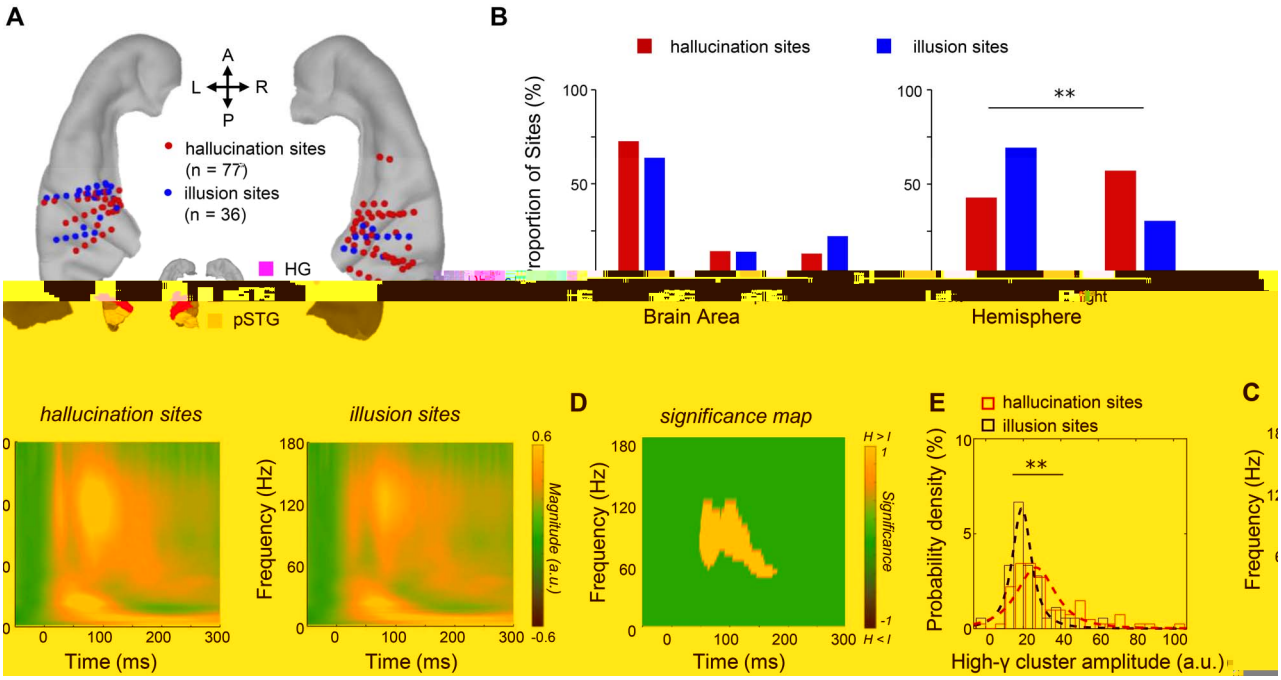

Fig. 2. Anatomical and time-frequency characteristics of hallucination and illusion sites. (A) Hallucination (*red*) and illusion (*blue*) sites are shown on the temporal lobe of the ICBM152 brain template. (B) Proportions of hallucination (*red*) and illusion (*blue*) sites in HG, mSTG, and pSTG (*left*) and in the left and right hemispheres (*right*). (C) Averaged time-frequency maps of sound-induced responses of hallucination sites (*left*) and those of illusion sites (*right*). (D) The statistical parametric map of time-frequency differences between sound-induced responses of hallucination sites and those of illusion sites. *Yellow areas* indicate significant time-frequency clusters ($P < 0.005$, *FDR* corrected). (E) Comparison of high-γ cluster (50–116 Hz; 49–139 ms) amplitudes between hallucination and illusion sites. *H: Hallucination; I: Illusion.* $^{**}P < 0.01$.

at hallucination and illusion sites (Fig. 2C). Our results revealed that the hallucination sites showed an early increase in power in the high-γ band (50–116 Hz) in response to the sounds, relative to the illusion sites ($P < 0.005$, *FDR* corrected) (Fig. 2D). Additionally, we observed that the mean amplitude of the early high-γ cluster was significantly larger in the hallucination sites than that in the illusion sites ($t\ (111) = 3.005$, $P = 0.003$; Fig. 2E). One possible explanation for this difference in high-γ amplitude is that the neuronal excitability of the hallucination sites is higher than that of the illusion sites. Here, we estimated the excitability of each site by defining the elicitation threshold as the minimum current intensity required to elicit a conscious percept (Fox et al. 2020). We found no significant difference between the averaged elicitation threshold of the hallucination sites (2.12 ± 1.22 mA; mean ± SD) and that of the illusion sites (2.07 ± 0.85 mA) ($t\ (111) = 0.267$, $P = 0.790$), demonstrating that different iES-elicited perceived contents cannot be explained by the neuronal excitability difference. Taken together, these findings show that the neuronal population corresponding to hallucination is characterized by an enhancement of sound-induced early high-γ activities.

We then employed binary logistic regression to examine whether the high-γ signatures we observed could predict the perceived contents (hallucination or illusion) elicited by iES. As illustrated in Fig. 1C, we constructed a binary logistic regression model using the amplitudes of discrete time-frequency bins within the high-γ range (50–116 Hz, 49–139 ms) extracted from sound-induced iEEG signals (Fig. 2D). Our analysis revealed that the high-γ band signatures extracted from iEEG responses to external sounds could predict 85.0% of the perceived contents (94.8% for hallucination, 63.9% for illusion) elicited by iES ($\chi^2\ (24) = 50.346$, $P = 0.001$).

We further categorized the hallucination and illusion sites based on the details of their perceived contents elicited by iES (Fig. 1A) (Trébuchon et al. 2021). We found that the majority of the hallucination sites (96.10%) exhibited simple sound percepts. In contrast, a dichotomy was observed among illusion sites, with 33.33% of the sites showing suppression perception and 66.67% of the sites showing echo perception. Most suppression and echo sites were localized in HG, with relatively smaller proportions in mSTG and pSTG (Fig. 3A and B). Regarding the proportions of the suppression and echo sites, there was no significant difference among HG, mSTG, and pSTG, suggesting a consistent distribution across the three areas ($\chi^2\ (2) = 2.010$, $P = 0.366$). No hemispheric asymmetry was observed either ($\chi^2\ (1) = 1.047$, $P = 0.306$).

We then compared the time-frequency maps of sound-induced responses in suppression and those in echo sites (Fig. 3C) and found that suppression sites showed an early high-γ activity (31–47 ms; 87–124 Hz) and a late γ activity (72–115 ms; 38–50 Hz) enhancement in response to sounds, relative to echo sites ($P < 0.005$, *FDR* corrected) (Fig. 3D). Both amplitudes of time-frequency clusters were significantly larger for suppression sites than for echo sites (high-γ cluster: $t\ (34) = 3.072$, $P = 0.004$; γ cluster: $t\ (34) = 3.146$, $P = 0.003$; Fig. 3E). We found no significant difference between the elicitation thresholds of suppression sites (1.79 ± 0.81 mA) and those of echo sites (2.21 ± 0.86 mA) ($t\ (34) = 1.397$, $P = 0.171$).

We built two binary regression models using the amplitudes of discrete time-frequency bins extracted from the high-γ range (87–124 Hz; 31–47 ms) and the γ range (38–50 Hz; 72–115 ms) (Fig. 3D) to predict perceived contents (suppression or echo), respectively. We found that the high-γ band signatures could predict 83.3% of perceived contents (suppression: 66.7%; echo: 91.7%) ($\chi^2\ (9) = 19.102$, $P = 0.024$), and the γ band signatures could predict 91.7% of perceived contents (suppression: 83.3%; echo: 95.8%) ($\chi^2\ (8) = 26.992$, $P = 0.001$). Together, these results demonstrate that high-γ and γ responses extracted from sound-induced iEEG

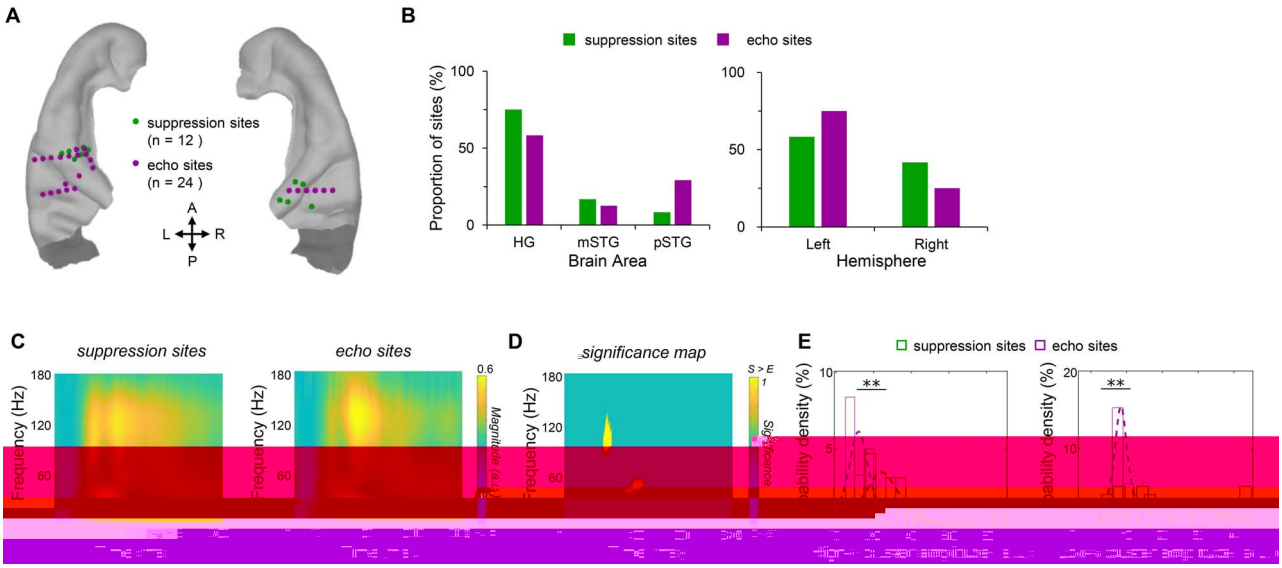

Fig. 3. Anatomical and time-frequency characteristics of suppression and echo sites. (A) Suppression (*green*) and echo (*purple*) sites are shown on the temporal lobe of the ICBM152 brain template. (B) Proportions of suppression (*green*) and echo (*purple*) sites in HG, mSTG, and pSTG (*left*) and the left and right hemispheres (*right*). (C) Averaged time-frequency maps of sound-induced responses of suppression (*left*) and those of echo (*right*) sites. (D) The statistical parametric map of time-frequency differences between sound-induced responses of suppression sites and those of echo sites. *Yellow areas* indicate significant time-frequency clusters ($P < 0.001$). (E) Comparison of a high-γ cluster (*left*; 87–124 Hz; 31–47 ms) and a low-γ cluster (*right*; 38–50 Hz; 72–115 ms) amplitudes between suppression (*green*) and echo (*purple*) sites. *Error bars* represent the standard error across sites. $^{**}P < 0.01$. S, suppression; E, echo.

signals can serve as powerful predictors of the perceived contents elicited by iES.

Intrinsic high-γ temporal profiles characterized iES-elicited perceived contents

Previous iEEG studies have shown that sound-induced high-γ responses can be classified into transient and sustained types based on their distinct temporal profiles (Hamilton et al. 2018; Yi et al. 2019; Forseth et al. 2020; Xu et al. 2023), suggesting the existence of functional dichotomy within neuronal populations characterized by distinct temporal profiles (Scott 2019). We also found that the iES-elicited perceived contents, including simple sound hallucinations and suppression/echo illusions, were associated with different sound-induced high-γ responses. Therefore, we investigated whether the diversity of iES-elicited perceived contents could be explained by the distinction of high-γ temporal profiles.

We applied convex NMF to the sound-induced high-γ responses averaged across trials (Li and Ngom 2013). As shown in Fig. 4A, we discovered two classes of responses that could explain 87.01% of the variance in the data: one with a strong response at the sound onset (transient), and the other with a long-lasting response (sustained). To compare the temporal properties of hallucination, echo, and suppression sites further, we calculated the relative weight of each site. For a given site, a higher relative weight value indicates a more transient response. Based on the comparison between the two NMF weights, we classified 27 transient sites (23.89%) and 86 sustained sites (76.11%) (Fig. 4B). Figure 4C shows that 70.4% of transient sites and 67.4% of sustained sites were engaged in hallucination. Moreover, transient sites were more frequently involved in the perception of suppression (22.0%), compared to their involvement in echo perception (7.4%) ($\chi^2(2) = 7.719$, $P = 0.021$). Figure 4D reveals that the relative weight of suppression sites was greater than that of echo sites ($t(34) = 2.588$, $P = 0.014$) and that of hallucination sites ($t(87) = 1.93$, $P = 0.057$). Additionally, we observed that the latency of suppression sites (21.16 ± 3.98 ms) was shorter than that of echo sites (41.59 ± 4.52 ms) ($t(34) = 2.915$, $P = 0.006$) and that of hallucination sites (32.92 ± 2.39 ms) ($t(87) = 1.879$, $P = 0.064$, *marginally significant*). These results indicate that the neuronal population engaged in suppression perception is characterized by rapid and transient sound-induced high-γ responses. Additionally, our findings elucidate the relationship between high-γ temporal profiles and subjective auditory experiences, offering empirical support for the functional dichotomy within neuronal populations possessing distinct temporal profiles, a concept hinted at by previous researches (Hamilton et al. 2018; Yi et al. 2019; Forseth et al. 2020; Xu et al. 2023).

Additionally, our analysis revealed a significant negative correlation between the medial-to-lateral coordinates and the relative weights of the intracranial sites ($r(113) = -0.326$, $P < 0.001$, *Pearson correlation test*). This suggests that sites positioned medially tend to exhibit more transient characteristics, whereas laterally placed sites show more sustained features. This finding regarding the anatomical distribution of a medial-to-lateral effect serves as an important complement to the anterior-to-posterior effect previously reported by Hamilton et al. (2018).

Sound-induced high-γ band signatures predicted perceived locations of hallucination sites

An iES-elicited auditory percept could be perceived either contralaterally or bilaterally to the stimulation side (Trébuchon et al. 2021; Jaroszynski et al. 2022). We observed that most of the hallucination and illusion sites were perceived contralaterally, while a small proportion of hallucination and illusion sites were perceived bilaterally (Fig. 1A).

To further investigate the differences between contralateral and bilateral hallucination sites, we analyzed their anatomical and time-frequency characteristics. As shown in Fig. 5A and B, compared with bilateral hallucination sites, more contralateral hallucination sites were located in the HG ($\chi^2(2) = 11.349$; $P = 0.003$). No hemispheric asymmetry was observed ($\chi^2(1) = 0.307$;

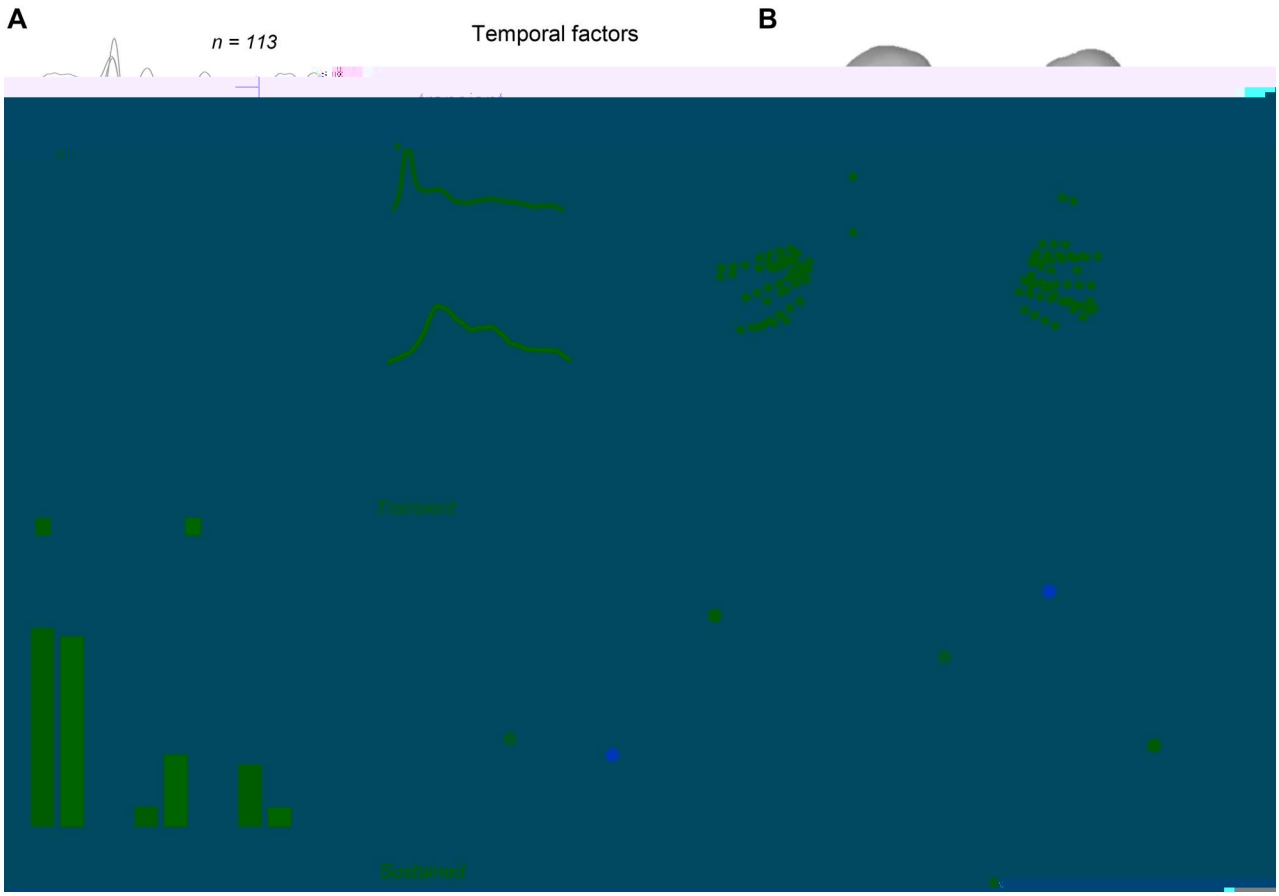

Fig. 4. High-γ temporal profiles and latencies of hallucination, echo, and suppression sites. (A) NMF clustering results for $k = 2$. Averaged high-γ responses were normalized and then entered into the clustering pool ($n = 113$). Two temporal factors were observed. One factor showed a strong response at sound onset (transient, *orange curve*), and the other showed a slow and sustained response (sustained, *yellow curve*). (B) Spatial distributions of transient (*orange*) and sustained sites (*orange*). (C) Proportions of transient (*orange*) and sustained (*yellow*) sites exhibited iES-elicited hallucination, echo, and suppression. (D) Comparison of relative activation weights for sites exhibiting iES-elicited hallucination, echo, and suppression perception. (E) Averaged first-significant latencies of hallucination, echo, and suppression sites. *Error bars* represent the standard errors across sites. W_T, transient weight; W_S, sustained weight. $^*P < 0.05$.

$P = 0.579$). Regarding time-frequency characteristics, we found that contralateral hallucination sites showed a late amplitude enhancement (107–158 ms) in the high-γ band (87–153 Hz) in response to sounds compared to bilateral hallucination sites ($P < 0.005$, *FDR* corrected) (Fig. 5C and D). The mean amplitude of the high-γ cluster of contralateral hallucination sites was significantly larger than that of bilateral hallucination sites ($t\,(64) = 2.732$, $P = 0.008$; Fig. 5E). No difference was found between the elicitation thresholds of contralateral hallucination sites (2.06 ± 1.21 mA) and bilateral hallucination sites (2.31 ± 1.30 mA) ($t\,(64) = 0.662$, $P = 0.510$). These results suggest that the neuronal population corresponding to contralateral hallucination is characterized by a late high-γ power enhancement in res.4(sponse.7(e)-.)-33(e)-.s6-1.4042T5a.4(higicouristed)-273.3(sound2364.on,)-240.3(m).stal(c)11

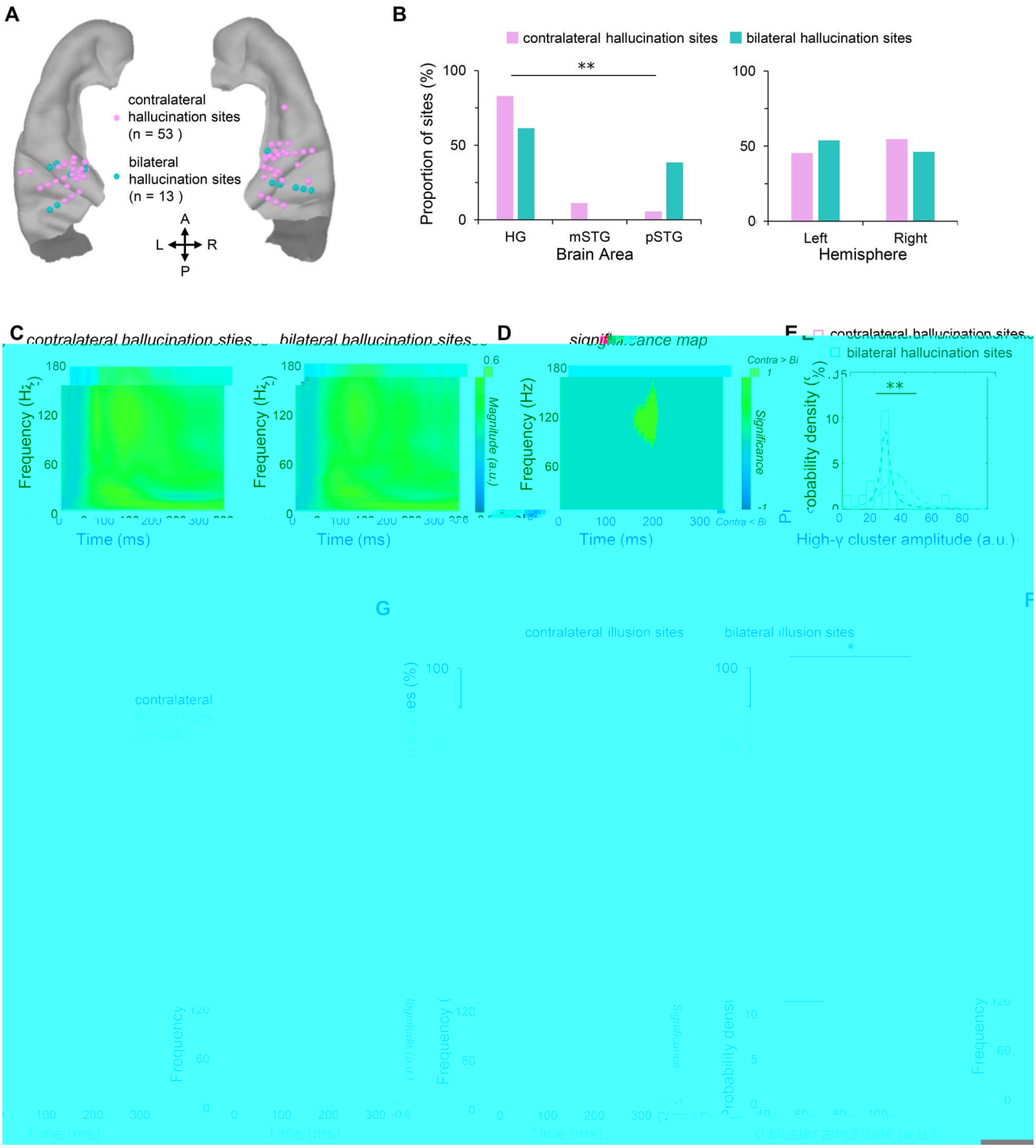

Fig. 5. Anatomical and time-frequency characteristics of sites with different iES-elicited perceived locations. (A) Contralateral (*pink*) and bilateral (*cyan*) hallucination sites are shown on the temporal lobe of the ICBM152 brain template. (B) Proportions of contralateral (*pink*) and bilateral (*cyan*) hallucination sites in HG, mSTG, and pSTG (*left*) and the left (a).7(nd)-372.5-he ().1(aemisphr)12.1(e) i()]TJ[illegible]

Overall, our findings suggest that the high-γ and α band signatures extracted from sound-induced iEEG can be used to predict perceived locations of hallucination and illusion sites, respectively.

Auditory space was differently represented in hallucination and illusion sites

Our findings that the perceived location elicited by stimulating hallucination sites and that of illusion sites could be determined by the sound-induced high-γ and α activities raise an interesting question: whether auditory space is represented differently in hallucination and illusion sites? To address this question, we presented ipsilateral and contralateral sounds to 22 patients (P236-P421) and analyzed a total of 77 sites divided into four groups (contralateral hallucination, bilateral hallucination, contralateral illusion, and bilateral illusion) (Fig. 6A). Time-frequency analyses were performed to extract spectra-temporal features in the high-γ and α bands for each site (Fig. 6B). We th
decoded the auditory space with single-trial sp
features using support vector machine approaches
out cross-validations. First, we trained and decode
space with single-trial spectra-temporal features in the high-γ band. Second, we trained and decoded the auditory space with the α band features. To compare the decoding accuracies among site groups, 2 (Perceived Location: contralateral, bilateral) × 2 (Perceived Content: hallucination, illusion) ANOVAs were performed for both high-γ and α models.

For the decoding accuracy using the high-γ band features, we found a significant main effect of Perceived Location ($F(1,73) = 7.921$, $P = 0.006$), indicating that auditory space was represented differently between contralateral and ipsilateral sounds. No significant effect of Perceived Content or interaction effect was found. Post hoc tests confirmed the Perceived Location effect in illusion conditions (contralateral hallucination vs. bilateral hallucination: $P = 0.067$; contralateral illusion vs. bilateral illusion: $P = 0.038$, Fig. 6C, left). For the α model, no significant main effects of Perceived Location ($F(1,73) = 2.605$, $P = 0.111$) or Perceived Content ($F(1,73) = 2.436$, $P = 0.123$) was found. No significant interaction effect was found. Post hoc tests showed that the decoding accuracy of contralateral illusion sites was higher than contralateral hallucination sites ($P = 0.041$, Fig. 6C, right).

We also compared the decoding accuracy using the high-γ and α band features in each site group. We found that the decoding accuracy using the α band features was higher than that of the high-γ band features in contralateral illusion ($t(17) = 3.668$, $P = 0.002$) and bilateral illusion ($t(7) = 2.126$, $P = 0.071$)) sites (Fig. 6E). No significant difference was found in contralateral hallucination or bilateral hallucination sites (both $P > 0.5$; Fig. 6D). These results suggest that the α band activity plays an essential role in representing auditory space in illusion sites.

In summary, our results encompass five critical findings: Firstly, sound-induced high-γ band signatures were instrumental in predicting the perceived contents elicited by iES. Secondly, the intrinsic temporal profiles of high-γ band activity distinctively characterized the perceived contents induced by iES. Thirdly, we found that the perceived locations of hallucination sites could be predicted by sound-induced high-γ band signatures. Fourthly,

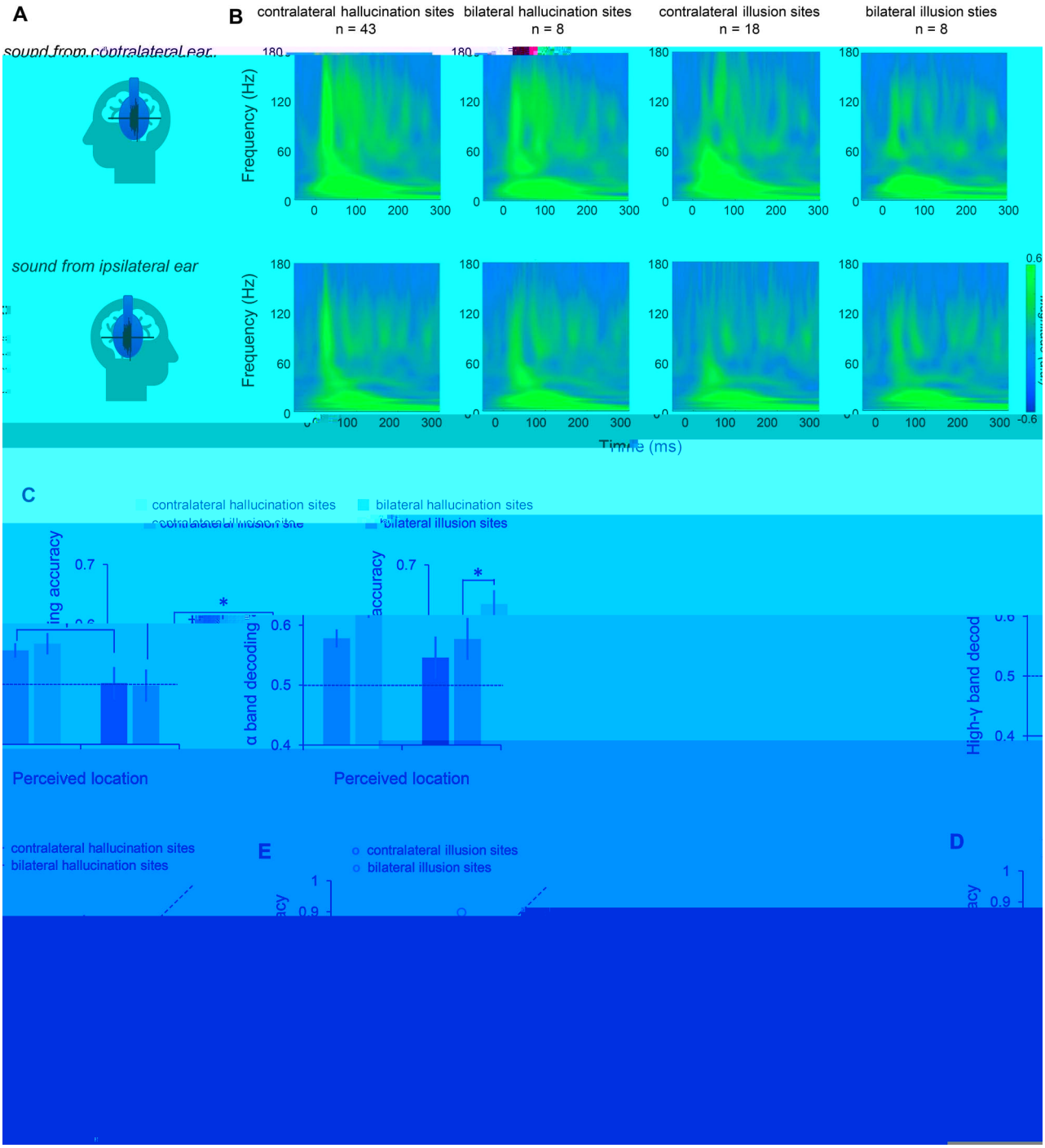

Fig. 6. Decoding accuracy of sites with different iES-elicited percepts. (A) Sounds were present either contralaterally or ipsilaterally. (B) Averaged time-frequency maps of neural signals responded to contralateral (*up*) and ipsilateral (*down*) sounds. (C), (D), (E) comparisons of decoding accuracies of the high-γ (*left*) and α (*right*) models. *$P < 0.05$; †$P < 0.1$.

information (Scott 2019), but empirical evidence for this relationship was lacking. Our findings supported this assumption by revealing that sites with different temporal response properties correspond to different perceived contents. Specifically, transient responses would be consistent with the motor-induced suppression of the auditory cortex, which is involved in perceptual guidance of action (Aliu et al. 2009; Ylinen et al. 2015), while sustained responses would be consistent with feedback influences on auditory object recognition processes (Scott 2019).

On the other hand, both hallucinations and illusions can be perceived contralaterally or bilaterally, based on their iES-elicited perceived locations (Fenoy et al. 2006; Jaroszynski et al. 2022). The current study established a relationship between high-γ and α band responses in the auditory cortex and perceived locations. Previous studies have found that both high-γ and α band signals can encode and characterize perceptual space (Bednar and Lalor 2018; Patel et al. 2018). Interestingly, in the current study, we found that hallucination sites and illusion sites encoded auditory space via high-γ and α band signals, respectively. We further revealed that auditory space information could be decoded from high-γ and α band time-frequency features, withα band features predominantly contributing to the decoding performance of illusion

sites. This finding is consistent with previous research that has shown that the α band plays an important role in illusions (Lange et al. 2014; Leske et al. 2014).

Furthermore, our study provides novel insights into the neural mechanisms underlying the formation of auditory illusions. The debate regarding the contributions of feedforward and feedback signals in illusion formation has been a major point of contention in the field (Samuel 1981; Gregory 1997; Bartlett et al. 2011). According to the hierarchical model, primary sensory cortex is responsible for hallucinations while high-order cortex is responsible for illusions (Halgren and Chauvel 1993; Howard et al. 2000; Fenoy et al. 2006). However, our results demonstrate that the distribution of illusion and hallucination sites along the auditory cortical hierarchy does not support this perspective. Instead, we found that a subset of illusion sites, specifically those responsible for suppression, exhibited a approximated response latency as that of the human primary auditory cortex (Nourski et al. 2014). Therefore, our findings support the idea that feedforward signals may play a primary role in generating illusions by directly modulating subjective experiences in humans.

Our findings may shed light on a promising avenue for treating various auditory-related neurological disorders. The auditory suppression effect induced by iES suggests a potential new approach for managing refractory tinnitus, as indicated by Fenoy et al. (2006). While tinnitus is often a consequence of damage to the peripheral auditory system (Jastreboff 1990; Roberts et al. 2010), the perceived severity of tinnitus is associated with specific cerebral activity patterns (Sedley et al. 2012, 2015; Norena and Farley 2013). Thus, it is conceivable that modulating these aberrant neural activities could alleviate tinnitus (De Ridder et al. 2004). The main challenge in such neuromodulation lies in pinpointing precise and effective cerebral targets for treatment (Vanneste and De Ridder 2012). Our study contributes to this field by identifying neuronal populations that exhibit heightened transient high-gamma activity in response to sound, which could serve as a potential biomarker for neuromodulation interventions in tinnitus therapy.

In sum, our study revealed that the neuronal response properties of different sites in the auditory cortex can effectively predict subjective sound experiences elicited by iES. This finding holds promising approach for the development of auditory cortical prostheses for individuals with acquired deafness. Additionally, our results may provide a novel direction for the treatment of other auditory-related neurological disorders.

Acknowledgments

We would like to express our heartfelt gratitude to Professor Xing Tian for his constructive comments on the initial draft of this paper. Additionally, we extend our sincere thanks to each patient and their family members who participated in this study. Their contributions were invaluable to the success of our research.

Author contributions

Qian Wang (Conceptualization, Data curation, Formal analysis, Funding acquisition, Investigation, Methodology, Writing—original draft, Writing—review & editing), Lu Luo (Data curation, Investigation, Methodology), Na Xu (Data curation, Investigation, Methodology), Jing Wang (Investigation, Methodology), Ruolin Yang (Investigation, Methodology), Guanpeng Chen (Investigation, Methodology), Jie Ren (Methodology), Guoming Luan (Methodology), and Fang Fang (Conceptualization, Investigation, Writing—review & editing)

Supplementary material

Supplementary material is available at *Cerebral Cortex* online.

Funding

This work was supported by the National Science and Technology Innovation 2030 Major Program (2022ZD0204802), and the National Natural Science Foundation of China (31930053) to F. F., the National Science and Technology Innovation 2030 Major Program (2022ZD0204804), the National Natural Science Foundation of China (32171039) and High-performance Computing Platform of Peking University to Q.W.

Conflict of interest statement: The author(s) declare that they have no conflict of interest.

Data availability

The data that support the findings of this study are available from the corresponding author, upon reasonable request.

References

Abeles M, Goldstein MH. Responses of single units in the primary auditory cortex of the cat to tones and to tone pairs. *Brain Res*. 1972:42(2):337–352.

Alain C, Arnott SR, Hevenor S, Graham S, Grady CL. "What" and "where" in the human auditory system. *Proc Natl Acad Sci*. 2001:98(21):12301–12306.

Aliu SO, Houde JF, Nagarajan SS. Motor-induced suppression of the auditory cortex. *J Cogn Neurosci*. 2009:21(4):791–802.

Bartlett EL, Sadagopan S, Wang X. Fine frequency tuning in monkey auditory cortex and thalamus. *J Neurophysiol*. 2011:106(2):849–859.

Bednar A, Lalor EC. Neural tracking of auditory motion is reflected by delta phase and alpha power of EEG. *NeuroImage*. 2018:181:683–691.

Bijanzadeh M, Khambhati AN, Desai M, Wallace DL, Shafi A, Dawes HE, Sturm VE, Chang EF. Decoding naturalistic affective behaviour from spectro-spatial features in multiday human iEEG. *Nat Hum Behav*. 2022:6(6):823–836.

Brugge JF, Reale RA, Hind JE. The structure of spatial receptive fields of neurons in primary auditory cortex of the cat. *J Neurosci*. 1996:16(14):4420–4437.

Chang CC, Lin CJ. LIBSVM: a library for support vector machines. *ACM transactions on intelligent systems and technology (TIST)*. 2011:2(3):1–27.

Cheung SW, Bedenbaugh PH, Nagarajan SS, Schreiner CE. Functional organization of squirrel monkey primary auditory cortex: responses to pure tones. *J Neurophysiol*. 2001:85(4):1732–1749.

De Graaf J, Liegeois-Chauvel C, Vignal J, Chauvel P. Electrical stimulation of the auditory cortex. In: Luders H, Noachtar S, editors. *Epileptic seizures: pathophysiology and clinical semiology*. New York: Churchill Livingstone; 2000. pp. 228–236.

De La Rocha J, Marchetti C, Schiff M, Reyes AD. Linking the response properties of cells in auditory cortex with network architecture: cotuning versus lateral inhibition. *J Neurosci*. 2008:28(37):9151–9163.

De Ridder D, De Mulder G, Walsh V, Muggleton N, Sunaert S, Møller A. Magnetic and electrical stimulation of the auditory cortex for intractable tinnitus: case report. *J Neurosurg*. 2004:100(3): 560–564.

Delorme A, Makeig S. EEGLAB: an open source toolbox for analysis of single-trial EEG dynamics including independent component analysis. *J Neurosci Meth*. 2004:134(1):9–21.

Dobelle W, Stensaas S, Mladejovsky M, Smith J. A prosthesis for the deaf based on cortical stimulation. *Ann Otol Rhinol Laryngol*. 1973:82(4):445–463.

Fenoy AJ, Severson MA, Volkov IO, Brugge JF, Howard MA III. Hearing suppression induced by electrical stimulation of human auditory cortex. *Brain Res*. 2006:1118(1):75–83.

Forseth KJ, Hickok G, Rollo P, Tandon N. Language prediction mechanisms in human auditory cortex. *Nat Commun*. 2020:11(1):5240.

Fox KC, Shi L, Baek S, Raccah O, Foster BL, Saha S, Margulies DS, Kucyi A, Parvizi J. Intrinsic network architecture predicts the effects elicited by intracranial electrical stimulation of the human brain. *Nat Hum Behav*. 2020:4(10):1039–1052.

Gregory RL. Knowledge in perception and illusion. *Philos Trans R Soc Lond Ser B Biol Sci*. 1997:352(1358):1121–1127.

Halgren E, Chauvel P. Experimental phenomena evoked by human brain electrical stimulation. *Adv Neurol*. 1993:63:123–140.

Hamilton LS. Human song: separate neural pathways for melody and speech. *Curr Biol*. 2022:32(7):R311–R313.

Hamilton LS, Edwards E, Chang EF. A spatial map of onset and sustained responses to speech in the human superior temporal gyrus. *Curr Biol*. 2018:28(12):1860–1871.e4.

Hamilton LS, Oganian Y, Hall J, Chang EF. Parallel and distributed encoding of speech across human auditory cortex. *Cell*. 2021:184:4626–4639.e13.

Howard MA, Volkov I, Mirsky R, Garell P, Noh M, Granner M, Damasio H, Steinschneider M, Reale R, Hind J. Auditory cortex on the human posterior superior temporal gyrus. *J Comp Neurol*. 2000:416(1):79–92.

Hsu CW, Chang CC, Lin CJ. *A practical guide to support vector classification*. Taiwan: Dep. of Computer Sci., National Taiwan University; 2003.

Jaroszynski C, Amorim-Leite R, Deman P, Perrone-Bertolotti M, Chabert F, Job-Chapron A-S, Minotti L, Hoffmann D, David O, Kahane P. Brain mapping of auditory hallucinations and illusions induced by direct Intracortical electrical stimulation. *Brain Stimul*. 2022:15(5):1077–1087.

Jastreboff PJ. Phantom auditory perception (tinnitus): mechanisms of generation and perception. *Neurosci Res*. 1990:8(4):221–254.

Joshi AA, Choi S, Liu Y, Chong M, Sonkar G, Gonzalez-Martinez J, Nair D, Wisnowski JL, Haldar JP, Shattuck DW. A hybrid high-resolution anatomical MRI atlas with sub-parcellation of cortical gyri using resting fMRI. *J Neurosci Methods*. 2022:374:109566.

Kaas JH, Hackett TA. 'What' and 'where' processing in auditory cortex. *Nat Neurosci*. 1999:2(12):1045–1047.

Lange J, Keil J, Schnitzler A, van Dijk H, Weisz N. The role of alpha oscillations for illusory perception. *Behav Brain Res*. 2014:271(100): 294–301.

Leonard MK, Baud MO, Sjerps MJ, Chang EF. Perceptual restoration of masked speech in human cortex. *Nat Commun*. 2016:7(1):13619.

Leske S, Tse A, Oosterhof NN, Hartmann T, Müller N, Keil J, Weisz N. The strength of alpha and beta oscillations parametrically scale with the strength of an illusory auditory percept. *NeuroImage*. 2014:88:69–78.

Li Y, Ngom A. The non-negative matrix factorization toolbox for biological data mining. *Source Code Biol Med*. 2013:8(1):10.

Mohan UR, Watrous AJ, Miller JF, Lega BC, Sperling MR, Worrell GA, Gross RE, Zaghloul KA, Jobst BC, Davis KA. The effects of direct brain stimulation in humans depend on frequency, amplitude, and white-matter proximity. *Brain Stimul*. 2020:13(5): 1183–1195.

Mullan S, Penfield W. Illusions of comparative interpretation and emotion: production by epileptic discharge and by electrical stimulation in the temporal cortex. *AMA Arch Neurol Psychiatry*. 1959:81(3):269–284.

Norena AJ, Farley BJ. Tinnitus-related neural activity: theories of generation, propagation, and centralization. *Hear Res*. 2013:295: 161–171.

Nourski KV, Steinschneider M, McMurray B, Kovach CK, Oya H, Kawasaki H, Howard MA III. Functional organization of human auditory cortex: investigation of response latencies through direct recordings. *NeuroImage*. 2014:101:598–609.

O'Sullivan J, Herrero J, Smith E, Schevon C, McKhann GM, Sheth SA, Mehta AD, Mesgarani N. Hierarchical encoding of attended auditory objects in multi-talker speech perception. *Neuron*. 2019:104(6):1195–1209.e3.

Otto KJ, Rousche PJ, Kipke DR. Microstimulation in auditory cortex provides a substrate for detailed behaviors. *Hear Res*. 2005:210 (1–2):112–117.

Patel P, Long LK, Herrero JL, Mehta AD, Mesgarani N. Joint representation of spatial and phonetic features in the human core auditory cortex. *Cell Rep*. 2018:24:2051–2062.e2.

Penfield W, Jasper H. *Epilepsy and the functional anatomy of the human brain*. Boston: Little Brown; 1954.

Penfield W, Perot P. The brain's record of auditory and visual experience: a final summary and discussion. *Brain*. 1963:86(4):595–696.

Penfield W, Rasmussen T. *The cerebral cortex of man; a clinical study of localization of function*. New York: Macmillan; 1950.

Rauschecker JP, Tian B. Mechanisms and streams for processing of "what" and "where" in auditory cortex. *Proc Natl Acad Sci*. 2000:97(22):11800–11806.

Roberts LE, Eggermont JJ, Caspary DM, Shore SE, Melcher JR, Kaltenbach JA. Ringing ears: the neuroscience of tinnitus. *J Neurosci*. 2010:30(45):14972–14979.

Rousche PJ, Otto KJ, Reilly MP, Kipke DR. Single electrode microstimulation of rat auditory cortex: an evaluation of behavioral performance. *Hear Res*. 2003:179(1–2):62–71.

Samuel AG. The role of bottom-up confirmation in the phonemic restoration illusion. *J Exp Psychol Hum Percept Perform*. 1981:7(5): 1124–1131.

Sani OG, Yang Y, Lee MB, Dawes HE, Chang EF, Shanechi MM. Mood variations decoded from multi-site intracranial human brain activity. *Nat Biotechnol*. 2018:36(10):954–961.

Scheich H, Breindl A. An animal model of auditory cortex prostheses. *Audiol Neurootol*. 2002:7(3):191–194.

Schrouff J, Raccah O, Baek S, Rangarajan V, Salehi S, Mourão-Miranda J, Helili Z, Daitch AL, Parvizi J. Fast temporal dynamics and causal relevance of face processing in the human temporal cortex. *Nat Commun*. 2020:11(1):656.

Scott SK. From speech and talkers to the social world: the neural processing of human spoken language. *Science*. 2019:366(6461): 58–62.

Sedley W, Teki S, Kumar S, Barnes GR, Bamiou DE, Griffiths TD. Single-subject oscillatory γ responses in tinnitus. *Brain*. 2012:135(10):3089–3100.

Sedley W, Gander PE, Kumar S, Oya H, Kovach CK, Nourski KV, Griffiths TD. Intracranial mapping of a cortical tinnitus system using residual inhibition. *Curr Biol*. 2015:25(9):1208–1214.

Sinha S, Crone N, Fotta R, Lenz F, Boatman D. Transient unilateral hearing loss induced by electrocortical stimulation. *Neurology*. 2005:64(2):383–385.

Tadel F, Baillet S, Mosher JC, Pantazis D, Leahy RM. Brainstorm: a user-friendly application for MEG/EEG analysis. *Comput Intell Neurosci*. 2011:2011:1–13.

Trébuchon A, Alario F-X, Liégeois-Chauvel C. Functional topography of auditory areas derived from the combination of electrophysiological recordings and cortical electrical stimulation. *Front Hum Neurosci*. 2021:15:702773.

Vanneste S, De Ridder D. Noninvasive and invasive neuromodulation for the treatment of tinnitus: an overview. *Neuromodulation Technol Neural Interface*. 2012:15(4):350–360.

Wang X. Neural coding strategies in auditory cortex. *Hear Res*. 2007:229(1–2):81–93.

Wang Q, Luo L, Wang J, Luan G. Color perception matches selectivity in human early visual cortex. *Brain Stimul*. 2020:13(1):253–255.

Xu N, Zhao B, Luo L, Zhang K, Shao X, Luan G, Wang Q, Hu W, Wang Q. Two stages of speech envelope tracking in human auditory cortex modulated by speech intelligibility. *Cereb Cortex*. 2023:33(5):2215–2228.

Yi HG, Leonard MK, Chang EF. The encoding of speech sounds in the superior temporal gyrus. *Neuron*. 2019:102(6):1096–1110.

Ylinen S, Nora A, Leminen A, Hakala T, Huotilainen M, Shtyrov Y, Mäkelä JP, Service E. Two distinct auditory-motor circuits for monitoring speech production as revealed by content-specific suppression of auditory cortex. *Cereb Cortex*. 2015:25(6):1576–1586.